Research Article

Pardis Ghahramani, Kamran Behdinan*, Rasool Moradi-Dastjerdi, and Hani E. Naguib*

Development and modeling of an ultra-robust TPU-MWCNT foam with high flexibility and compressibility

https://doi.org/10.1515/ntrev-2023-0219
received December 10, 2022; accepted February 21, 2024

Abstract: Developing a cost-effective industrially scalable manufacturing method that can improve the mechanical properties of nanocomposite foams with higher flexibility, compressibility, and, at the same time, mechanically robustness is of significant interest. In this study, porous thermoplastic polyurethane (TPU)/multiwalled carbon nanotube (MWCNT) was fabricated with the chemical blowing agent (CBA) by a combination of compounding-compression molding methods. The effects of CBA and MWCNT contents on the foam morphology, porosity, foam cell size, Young's modulus, and compressibility of fabricated samples were investigated. Through conducting cyclic compressive tests, it was observed that nanocomposite foams exhibited consistent mechanical responses across multiple compressive cycles and demonstrated notable characteristics, including high compressibility (up to 76.4% compressive strain) and high elastic modulus (up to 8.8 ± 2.6 MPa). Moreover, theoretical approaches were employed to predict the elastic modulus of solid and foam TPU/MWCNT. For solid MWCNT/TPU, a specific micromechanical model based on different modifications of the Halpin-Tsai (HT) approach was used, which showed a good agreement with experimental data at different MWCNT contents. Furthermore, the constant parameters of Gibson and Ashby's method were found to successfully predict the elastic modulus of foam TPU/MWCNT at different MWCNT and CBA percentages.

Keywords: chemical blowing agent, experimental characterization, theoretical modeling, elastic modulus, TPU/MWCNT nanocomposite

1 Introduction and background

In recent years, flexible strain sensors with their potential prospects have attracted great attention [1–5] in many fields. These fields include wearable electronics such as stretchable materials for electronic devices [6,7], wearable sensors [8], energy harvesters [9,10], and micropumps with active diaphragms [11]; field of human movement monitoring [12,13], soft robotics for elastomer actuators [14] or self-healing actuators [15], sensitive electronic skin [16], and prosthetics [17,18]. Piezoresistive nanocomposite foams consisting of conductive nanoparticles and a flexible polymeric matrix are one of the significant types of flexible strain sensors [19–21]. This type of sensor provides tremendous advantages, such as high electrical conductivity, high flexibility, compressibility, and lightweight [22]. The sensing mechanism of piezoresistive foam nanocomposites is based on the electrical resistance variation in response to applied external stress [23,24].

Foaming the nanocomposites can enhance their electrical properties [25] and tailor their mechanical properties, including flexibility [26,27], compressibility [28], and mechanical strength [29,30]. The mechanical properties of nanocomposite foam sensors are crucial for their design and development, in addition to the electrical properties. Pressure-detecting sensors must be both flexible and compressible when subjected to high-pressure loads, without compromising their morphology, durability, and mechanical strength. While the addition of conductive

* **Corresponding author: Kamran Behdinan**, Advanced Research Laboratory for Multifunctional Lightweight Structures (ARL-MLS), Department of Mechanical & Industrial Engineering, University of Toronto, Toronto, Canada, e-mail: Behdinan@mie.utoronto.ca
* **Corresponding author: Hani E. Naguib**, Toronto Smart Materials and Structures (TSMART), Department of Mechanical & Industrial Engineering, University of Toronto, Toronto, Canada, e-mail: Neguib@mie.utoronto.ca
Pardis Ghahramani: Advanced Research Laboratory for Multifunctional Lightweight Structures (ARL-MLS), Department of Mechanical & Industrial Engineering, University of Toronto, Toronto, Canada; Toronto Smart Materials and Structures (TSMART), Department of Mechanical & Industrial Engineering, University of Toronto, Toronto, Canada
Rasool Moradi-Dastjerdi: Advanced Research Laboratory for Multifunctional Lightweight Structures (ARL-MLS), Department of Mechanical & Industrial Engineering, University of Toronto, Toronto, Canada

reinforcements can aid in the formation of conductive paths in the insulating polymer matrix, excessive filler content can harm the mechanical properties of the nanocomposite foam, reducing its processability and limiting its potential applications [31]. Despite successful demonstrations of nanocomposite foam sensors reported in the literature, they still have some limitations [32]. These sensors have low Young's modulus, limited recoverability, weak compressive strength, and a restricted pressure detection range of up to 900 kPa [1,33–37]. Yao *et al.* [38] showed that the detection range of polyurethane–graphene sponges was as low as 10 kPa, indicating its poor mechanical strength. Some nanocomposite foams are insensitive to large strain levels (more than 30%) due to conductive network saturation [39]. Additionally, fabricating a piezoresistive nanocomposite foam with a controlled elastic modulus that can operate within a broad loading range at a limited thickness is challenging [40,41].

Moreover, developing a cost-effective and scalable fabrication technique to create nanocomposite foams with uniformly distributed conductive fillers and controlled porosity, cell wall thickness, and foam morphology for achieving superior mechanical properties in the foam structure is a critical objective. Many foaming fabrication methods such as the particulate leaching method [42,43] are not cost-effective and scalable to the industrial manufacturing process. Supercritical gas foaming is an environmentally friendly industrial-scale technique that creates porous structures in thermoplastic polymeric (TPU) matrixes. However, in the nanocomposites with high loadings of nanoparticles, the gas diffusion is decreased, which adversely affects the physical foaming process and reduces the expansion ratio of the foamed product [26,44]. Also, the physical blowing agent (PBA) requires high pressure to be dissolved in the polymeric phase, which limits some types of foaming processes that are not practical at high pressures [45]. Hence, to broaden the nanocomposite foam applications, a new strategy that is able to enhance its mechanical properties with high controllability *via* an industrially scalable method is of great interest. One possible alternative foaming technique is implementing chemical blowing agent (CBA) particles, which promise highly controllable foaming with a uniform close-cell structure [1,46]. When subjected to heat, CBA thermally decomposes and produces gas, which can be trapped inside the polymeric matrix and create a foam structure [47]. CBA content and decomposition rate have a significant role in the foaming process of polymeric mixtures [48]. Unlike PBA, CBA particles operate at the pressure-free operating condition and undergo the chemical reaction at the decomposition temperature, which makes them a proper candidate to be utilized in pressure-free foaming processes such as rotational foam molding [45]. Therefore, compared to PBAs, CBAs are easier to handle and have more engineering and economic efficiency [47].

The design parameters including the polymer matrix, porous structure, characteristics of conductive filler, and manufacturing technique significantly impact the electrical and mechanical properties of nanocomposite foams. Despite existing literature on the topic, currently, a comprehensive study investigating the impact of foam porosity and morphology, filler contents, and sample fabrication methods on piezoresistivity, repeatability, and mechanical properties of nanocomposite foam sensors is missing [35,49]. Therefore, more research in this field is necessary to consider all these factors. In the current study, TPU was used as the polymeric phase due to its beneficial properties, which expand its application in a variety of fields. TPU is a flexible material that suits our target for compressibility in this study [41,50]. Moreover, it has abrasion resistance, chemical resistance, and ease of processing due to being melt-processable and recyclable [26,51]. Having high mechanical and electrical properties including high conductivity, large aspect ratio, and high elastic modulus, multiwalled carbon nanotube (MWCNT) was chosen as the nanofiller in this study [52–55].

In this work, TPU/MWCNT foam nanocomposites with varying contents of MWCNT and CBA were fabricated, and their flexibility, compressibility, and mechanical properties were analyzed. Moreover, the effects of nanofiller and blowing agent contents on the foam porosity, morphology, and mechanical properties of TPU/MWCNT nanocomposites were investigated. The potential application of fabricated TPU/MWCNT nanocomposite foams is in pressure-detecting systems to help the rehabilitation of people with artificial joints and suffering from osteoarthritis [56,57]. Unbalanced pressure distribution applied to the artificial knee over time can cause the wear of the tibial insert and result in further problems [58]. Pressure-detecting sensors embedded in artificial knees can detect plantar pressure map which shows the pressure distribution applied to the knee. The recorded results from the pressure sensors will be used to detect the accuracy and further adjustment of the designed biomechanical system.

Due to the limitations and costs associated with experimental tests, theoretical models are also used in our research to predict Young's modulus of solid and foam nanocomposites. This approach offers a better understanding of material properties and helps identify the ideal conductive reinforcement content, which can meet the desired mechanical property requirements [59]. Therefore, in this study, Young's modulus of solid TPU/MWCNT nanocomposites was predicted by micromechanical models

based on several modified HS approaches. Also, based on experimental results, the constant parameters of Gibson and Ashby's method for evaluating Young's modulus of foams made of pure TPU or MWCNT/TPU nanocomposites were proposed.

2 Experimental section

2.1 Experimental materials

TPU (Estane 58202, an 85A polyether-type thermoplastic polyurethane) was purchased from the Lubrizol Corporation. The CBA, azodicarbonamide (AC or ADCA) (CELLCOM-AC3000FD, decomposition temperature of 201–205°C), was ordered from Kum Yang Company Limited. The MWCNT (NC7000^{TM} series, average length of 1.5 mm, average diameter of 9.5 nm) was purchased from Nanocyl Company. All materials were used in the sample fabrication as received without further modifications.

2.2 Manufacturing process of TPU nanocomposites and their foams

Fabrication of TPU/MWCNT foams involved two different stages. One stage was blending the materials with the micro-compounder (DSM Xplore, MICRO 15, The Netherlands) to create homogeneous filaments. The second stage involved using the hot press compression molding (Carver Model 4386, USA) to reshape the filaments and create the samples with the desired shape, which was suitable for characterization. Since the CBAs are temperature sensitive, these particles should not be activated during the blending process. Otherwise, during the compression molding process, due to the extra heat and high pressure, their structure will be damaged, and porous morphology will not be achieved. Therefore, during the blending stage, the operating temperature was selected far from the CBA decomposition temperature (higher than TPU's melting point [155°C]) to just create solid TPU/CBA/MWCNT filaments. Later, in the compression molding stage, by increasing the working temperature, CBAs could decompose and create a porous structure.

Figure 1 shows the manufacturing process of TPU/MWCNT foams. At the beginning of this process, the specified weight ratios of TPU pellets and CBAs were fed to the micro-compounder through the conical forced feeding part. At this stage (the first step of compounding), materials were blended for 2.5 min with a speed of 200 rpm and a working temperature of 160°C. Then, the obtained filament was cut into small pieces for step 2 of compounding, and at this time, different weight ratios of MWCNTs were added to TPU/CBA pieces. It is worth mentioning that blending the MWCNTs at the same time with the TPU pellets and CBAs hindered the CBAs from being activated completely by heat in the compression molding stage. The reason for this phenomenon could be the entanglement of MWCNTs with TPU, which caused improper mixing of CBAs with TPU. Therefore, two-step compounding was conducted to create TPU/CBA/MWCNT solid filaments. In compounding step 2 similar operating condition as the first step was used. In the next stage, obtained TPU/CBA/MWCNT solid filaments were cut into small pieces and were filled into an

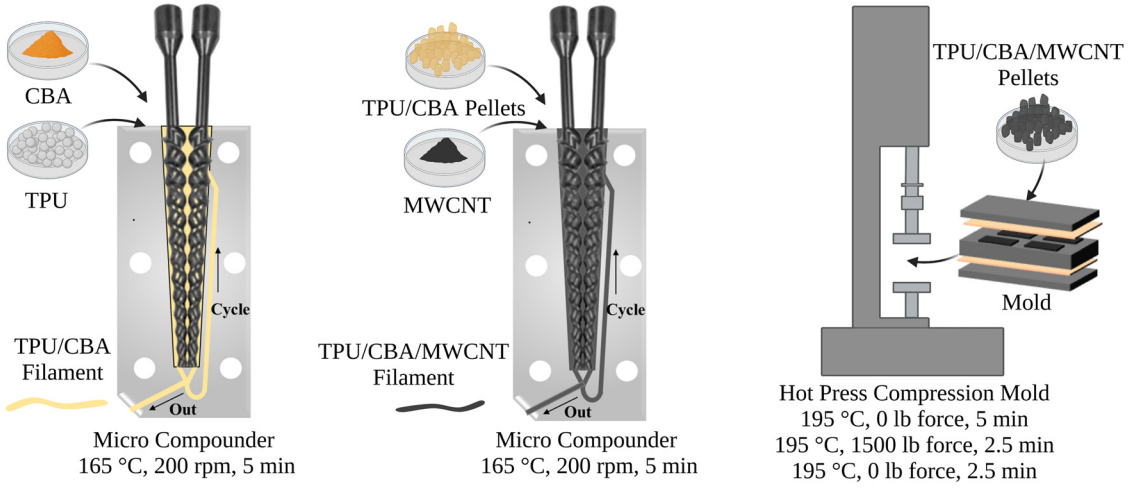

Figure 1: Schematic of foam TPU/MWCNT manufacturing process.

Table 1: Composition of fabricated samples

Sample identification	MWCNT content (wt%)	CBA content (wt%)
N0-F0, N0-F3, N0-F5	0	0, 3, 5
N1-F0, N1-F3, N1-F5	1	0, 3, 5
N3-F0, N3-F3, N3-F5	3	0, 3, 5
N5-F0, N5-F3, N5-F5	5	0, 3, 5

aluminum mold with rectangular cuboid cavities (25.0 mm [L] × 12.5 mm [W] × 2.0 mm [T]). Then, the mold was transferred into the hot press compression molding with a preset temperature of 195°C. Once the mold was in contact with both heating platens of the device, it was heated up for 5 min without external pressure. After 5 min, the mold was pressurized to 1,000 psi for 2.5 min. Then, in order to provide space for the expansion of CBAs, the external pressure was released to zero while the mold was in contact with two heating plates for an additional 2.5 min. Afterward, the mold was removed from the hot press compression molding and instantly cooled with cold water. Once the samples were removed from the mold cavities, they were placed in an oven to dry at 70°C for 24 h. TPU foam samples were fabricated with the manufacturing process shown in Figure 1 with the only difference of excluding step 2 of compounding since MWCNTs were not used for this type of sample. Also, the fabrication process of solid TPU/MWCNT nanocomposite followed the same procedure as TPU/MWCNT foams, excluding the first step of compounding. The final products with various MWCNT and CBA contents are named as summarized in Table 1. In this table, Nn-Fm indicates a sample that has n wt% MWCNT content and m wt% CBA content.

2.3 Characterization methods

Cyclic compression tests were carried out on an Instron 5944 machine (Instron, Norwood, USA-2kN load cell) with a displacement rate of 1 mm/min and a maximum allowable force of 1.9 kN in ten continuous loading–unloading cycles [41,60–62]. The average sample geometry was 25.0 mm (L) × 12.5 mm (W) × 2.0 mm (T). Young's modulus of the samples was determined through a linear regression analysis of the compressive stress versus compressive strain curves, focusing on the initial 5% of the compressive strain in the first loading cycle. The slope of the resulting trendline was used as the calculated value for Young's modulus.

A scanning electron microscope (SEM, JSM-IT100, InTouch Scope™, JOEL Inc, Tokyo, Japan) at 10 kV was used to observe the morphologies of the fabricated foams. For SEM sample preparation, foams were submerged in liquid nitrogen to be cryo-fractured. Then, the fractured cross-sectional surface was subjected to the sputter-coating device (DII-29010SCTR Smart Coater, JOEL Inc, Tokyo, Japan) for 4 min.

The average cell diameter of nanocomposite foams was assessed through the analysis of SEM micrographs using ImageJ software [63–65].

3 Theoretical approaches

To estimate the elastic modulus of the fabricated TPU/MWCNT foams at any MWCNT or porosity percentages, a theoretical approach has been developed. In this approach, in the first step, the elastic modulus of solid TPU/MWCNT nanocomposites is calculated at various MWCNT contents using micromechanical models based on the Halpin-Tsai (HT) approach. Then, using the results of the previous step, the elastic modulus of foams made of pure TPU or TPU/MWCNT nanocomposites is evaluated. In the second step, a method introduced by Gibson and Ashby [66] is used to calculate the elastic modulus ratio of foams to their solid material at any porosity percentage.

3.1 Solid TPU/MWCNT

To utilize this heavily employed approach for nanocomposite materials, various modifications to the original HT have been performed. In MWCNT-reinforced nanocomposites, there are a few parameters that affect the mechanical properties of the resulting nanocomposites such as the aspect ratio, agglomeration, orientation, and waviness of CNTs [67–69]. To capture the effect of MWCNT aspect ratio (AR) when they are dispersed with random orientations, the elastic modulus of such nanocomposites E_{nc} can be estimated as a function of longitudinal E_L and transverse E_T components of the elastic modulus as follows [70,71]:

$$E_{nc} = \frac{3}{8}E_L + \frac{5}{8}E_T, \tag{1}$$

where the definition of E_L and E_T are given as follows [70,71]:

$$E_L = \frac{1 + \mathrm{AR} \cdot \eta_L . f_r}{1 - \eta_L . f_r}E_m, \quad E_T = \frac{1 + 2\eta_T . f_r}{1 - \eta_T . f_r}E_m, \tag{2}$$

where f_r is MWCNT volume fraction and

$$\mathrm{AR} = \frac{l_{\mathrm{CNT}}}{d_{\mathrm{CNT}}},\quad \eta_{\mathrm{L}} = \frac{(E_r/E_m) - 1}{(E_r/E_m) + \mathrm{AR}},\quad \eta_{\mathrm{T}} = \frac{(E_r/E_m) - 1}{(E_r/E_m) + 2}, \tag{3}$$

where l_{CNT}, d_{CNT}, E_r, E_m are MWCNT length, MWCNT diameter, elastic modulus of the reinforcement (*i.e.*, MWCNT), and elastic modulus of the matrix (*i.e.*, TPU), respectively.

Considering the geometrical shape of the reinforcement components, the coefficients of E_{L} and E_{T} in equation (1) are also suggested to be as follows [72]:

$$E_{\mathrm{nc}} = \frac{2}{10}E_{\mathrm{L}} + \frac{8}{10}E_{\mathrm{T}}. \tag{4}$$

To further involve the effect of reinforcement waviness and distribution states, another modified HT approach has been introduced, as mentioned in the following equation [73,74]:

$$E_{\mathrm{nc}} = \frac{1 + 2\mathrm{AR}\cdot\eta.\, f_r}{1 - \eta.\, f_r}E_m, \tag{5}$$

where

$$\eta = \frac{(F_O \cdot F_W \cdot F_A \cdot E_r/E_m) - 1}{(F_O \cdot F_W \cdot F_A \cdot E_r/E_m) + 2\mathrm{AR}}. \tag{6}$$

F_O, F_W, and F_A represent orientation, waviness, and agglomeration factors of MWCNTs, respectively.

The orientation factor is applied to consider the effect of random orientations of MWCNTs, as $F_O = 1$ assumes that all MWCNTs are oriented in the same direction. The use of $F_O = 1/3$ and $F_O = 1/6$ has been recommended for two-dimensional and three-dimensional random orientations, respectively [73–75]. As 3D distribution for MWCNTs has been considered, in this work, $F_O = 1/6$ was selected for the orientation factor.

Due to MWCNT's high aspect ratio, they are usually bent when they are added to their matrix material. Therefore, a waviness factor, which is defined based on an assumed wave shape of long MWCNTs, has also been considered to capture the effect of MWCNT's bending in the HT approach. As suggested in previous studies [73,76,77], $F_W = 0.6$ is selected to modify the HT model introduced in equation (5).

Moreover, to better modify the evaluation of the elastic modulus of the nanocomposite, an agglomeration factor is suggested to modify the utilized HT approach in equation (7) as follows [73,74]:

$$F_A = \exp(-\alpha f_r^{\beta}), \tag{7}$$

where α and β are two coefficients that define various agglomeration states of MWCNTs.

Finally, to bridge MWCNT content from weight fraction wt to volume fraction, the following equation can be employed:

$$f_r = \frac{\mathrm{wt}}{\mathrm{wt} + \frac{\rho_r}{\rho_m} - \frac{\rho_r}{\rho_m}\mathrm{wt}}, \tag{8}$$

where ρ_r and ρ_m are the mass density of MWCNT and TPU.

3.2 TPU and TPU/MWCNT foams

According to Gibson and Ashby's method [66], the elastic modulus of foam is a function of density ratio $\lambda = \rho_f/\rho_s$ where the subscripts of f and s indicate a property attributed to foam and solid (non-porous) made of the same material, respectively. They suggested the following equation to estimate the relative elastic modulus of foams based on density ratio [66,78]:

$$E_f/E_s = C\lambda^n, \tag{9}$$

where C and n are two constants that can be defined by performing regression analysis on the experimental data. These constants are changed by void geometry, foam material, cell type, etc.

It is worth mentioning that the following equation shows the relation between density ratio and porosity percentage γ, which is usually utilized to identify the amount of porosity in foams [62,63]:

$$\gamma = (1 - \lambda) \times 100\%. \tag{10}$$

Accordingly, for example, $\gamma = 0\%$ and $\gamma = 40\%$ represent a non-porous material ($\lambda = 1$) and a foam in which 40% of its volume fraction is occupied with porosities ($\lambda = 0.6$).

4 Results and discussion

Figure 2 presents the cyclic compression test curves (ten cycles) for the fabricated samples with different contents of MWCNTs and CBAs. Furthermore, this figure presents a focused area of an initial 5% of the compressive strain in the first loading cycle for each sample. Young's modulus of the samples is calculated based on linear regression analysis of the compressive stress versus compressive strain curves of this section. The curves in Figure 2 indicate that all the samples follow a repeatable mechanical behavior in

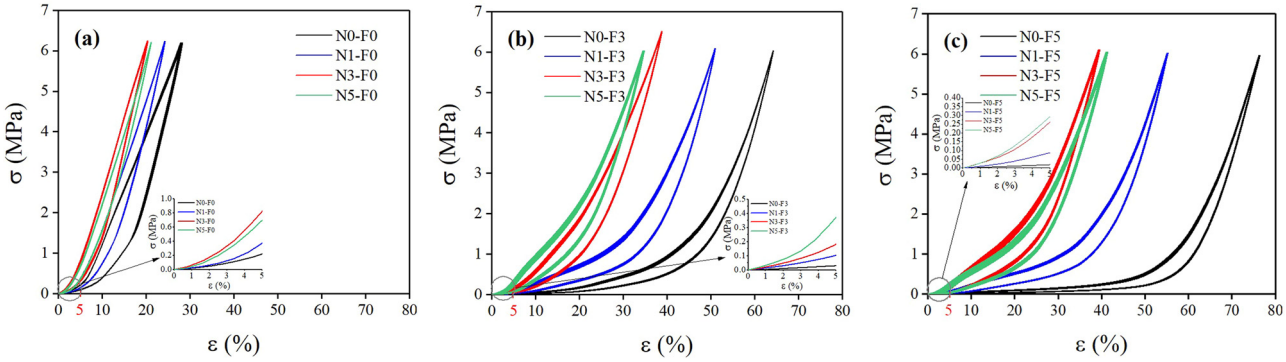

Figure 2: 10 cyclic compression test curves. (a) solid TPU and TPU/MWCNT, (b) foam TPU and TPU/MWCNT with 3 wt.% CBA, and (c) foam TPU and TPU/MWCNT with 5 wt.% CBA.

Table 2: Maximum strain levels under force of 1,900 N

MWCNT (wt%)	0 wt% CBA	3 wt% CBA	5 wt% CBA
0	27.8	64.3	76.4
1	24.2	51.0	55.3
3	20.4	38.9	39.6
5	21.2	34.9	41.4

different compression cycles. Moreover, this figure shows that the inclusion of CBAs in the polymer matrix increased the sample's flexibility and elevated their strain range under compression test. Based on the data plotted in Figure 2, it is evident that the inclusion of MWCNTs in the foam structures has a significant impact on their compressibility and maximum strain capacity. Table 2 presents a concise overview of the maximum strain capacity exhibited by different categories of nanocomposite foams when subjected to a uniform force range. As per Table 2, in comparison with the pristine foams (N0-F3 and N0-F5), the inclusion of 1 wt% MWCNT in N1-F3 and N1-F5 samples reduced their maximum strain by 13.3 and 21.1%, respectively. Also, increasing the MWCNT content to 3 wt% in N3-F3 and N3-F5 had a similar impact on their compressibility and the maximum strain that they could undergo. The maximum strain in N3-F3 and N3-F5 was further reduced by 25.4 and 36.8% compared to their pristine foams.

Figure 3(a) presents Young's modulus of solid TPU, solid TPU/MWCNT with different MWCNT weight ratios, TPU foams with different CBA contents, and TPU/MWCNT foams with different MWCNT and CBA contents. This figure demonstrates that the foam TPU and TPU/MWCNT have considerably lower Young's modulus compared to the solid TPU and TPU/MWCNT. This reduction in Young's modulus is attributed to the inclusion of CBAs in the polymer matrix, which introduces a porous structure to the morphology of the samples, resulting in increased flexibility but decreased mechanical strength [61]. However, it is

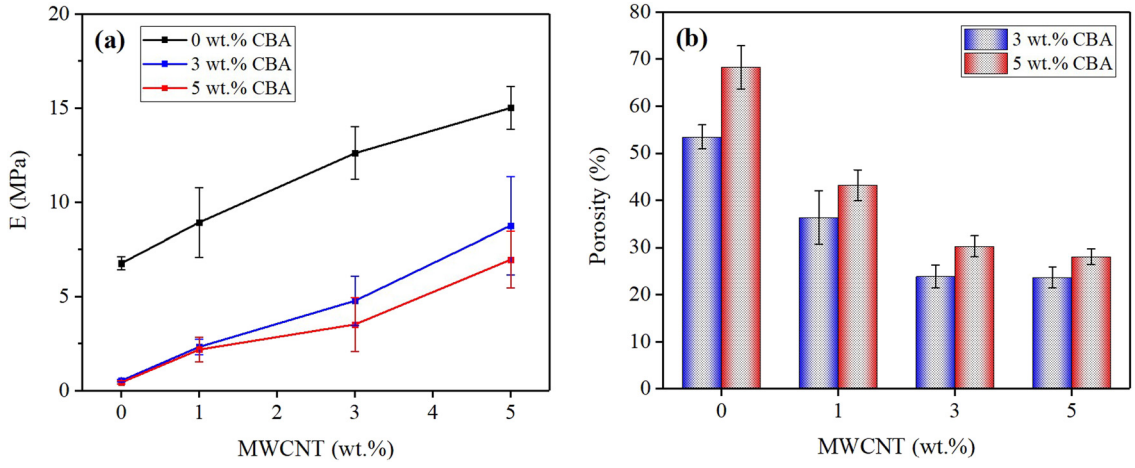

Figure 3: (a) Young's modulus of TPU, TPU/MWCNT solid, and foamed nanocomposites, (b) porosity of foamed TPU and TPU/MWCNT at different CBA and MWCNT contents.

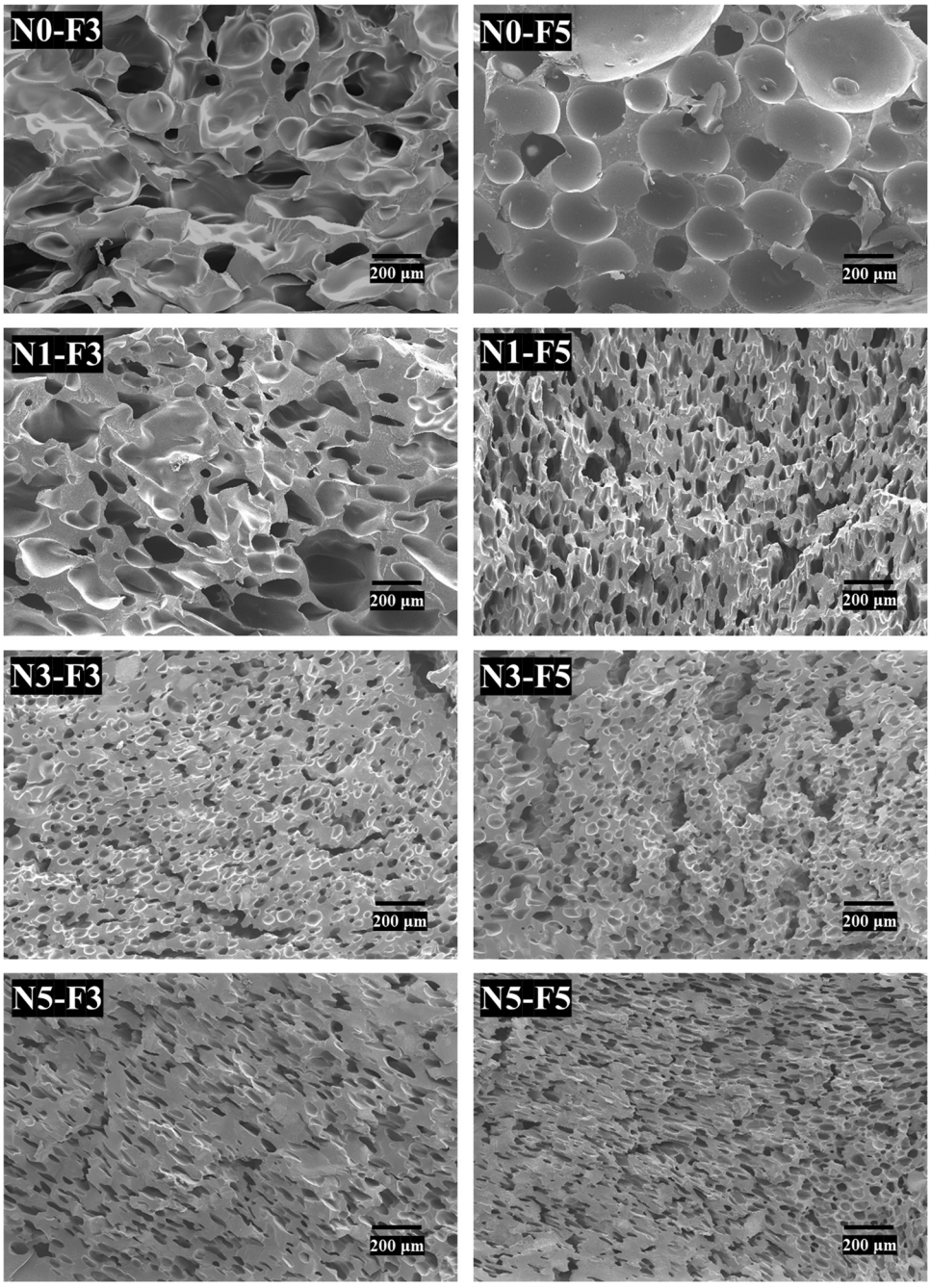

Figure 4: Cellular morphology of foamed TPU and TPU/MWCNT at different CBA and MWCNT contents.

noteworthy that the foams fabricated in this study exhibit significantly enhanced mechanical strength compared to similar foams reported in the literature [39]. Moreover, Figure 3(a) shows that increasing the MWCNT content, increased Young's modulus of both foam and solid samples in a similar trend. The high elastic modulus of MWCNTs contributes to the enhancement of mechanical strength observed in nanocomposite structures [42,43]. Moreover, the results revealed that N0-F3 demonstrated a higher Young's modulus of 527 ± 80 kPa in comparison to N0-F5 with a Young's modulus of 430 ± 78 kPa. Figure 3(b) illustrates the porosity characteristics of both foamed TPU and TPU/MWCNT samples. As depicted in this figure, an increase in the content of CBAs in nanocomposite foams with 5 wt% CBA resulted in higher porosity compared to the ones containing 3 wt% CBA. This increase in porosity resulted in enhanced flexibility and softness, consequently leading to reduced mechanical strength and Young's modulus [63,64].

As depicted in Figure 3(b), the introduction of MWCNTs into the polymer matrix resulted in a reduction in the foam porosity of the nanocomposite foams containing both 3 and 5 wt% CBAs, as the MWCNT content was increased up to 3 wt%. This phenomenon could be attributed to the entanglement of MWCNTs with CBAs, which hindered the proper dispersion of CBAs within the polymer matrix and limited cell formation.

However, the porosity change was found to be negligible when the MWCNT content was further increased from 3 to 5 wt%, as per the obtained results. SEM micrographs with uniformly porous structures in Figure 4 confirm the results of porosity measurements. According to these micrographs, N0-F3 and N0-F5 samples had a larger number of voids with larger cell sizes in their structure. This revealed that increasing the CBAs weight ratio resulted in the growth of porosity in the N0-F5 sample due to the higher gas production during blowing agent decomposition. Moreover, the SEM micrographs show that as MWCNT content increased in the foam structures, smaller cells appeared in their morphology. Figure 5 summarizes the average cell size of different types of foams. The presence of MWCNTs with their fine dimensions and large surface area in the nanocomposite structure created more challenges for bubble growth within the polymer matrix, which led to reduced cell sizes. However, at large MWCNT contents, the average cell sizes in TPU/MWCNT foams with 3 and 5 wt% MWCNT were statistically equal [79]. Considering the results of Figures 3 and 5, it can be comprehended that, alongside the higher MWCNT content and reduced porosity, smaller foam cell sizes could contribute to the sample's stiffness, thereby resulting in an elevated value of Young's modulus.

4.1 Theoretical characterization

As already mentioned in Section 3, the developed theoretical method starts with the characterization of solid TPU/MWCNT nanocomposites. The comparison between the average experimental results performed in this article and HT approaches presented in equations (1), (4), and (5) indicates which HT approach has the best level of accuracy in the elastic modulus estimation of such solid nanocomposites. As shown in Figure 6, equation (1) offers better estimations in comparison with equation (4). However, at a higher amount of MWCNT contents, they both fail in the estimation of the elastic modulus of solid TPU/MWCNT nanocomposites as they consider a steady increase of elastic modulus with the increase of CNT volume fraction, which cannot practically happen.

Due to the involvement of more MWCNT parameters in the estimation of elastic modulus, it can be seen that equation (5) offers the best estimations when the coefficients of the agglomeration factor (*i.e.*, α and β) are properly selected. It is shown that equation (5) with $F_O = 1/6$, $F_W = 0.6$, $\alpha = 7$, and $\beta = 0.085$ successfully estimates the elastic modulus such that this estimation either crosses the average values of experimental data or it is within the standard deviation experimental values. Moreover, it is shown that this approach is relied on the correct selection of α and β such that the selection of other combination values of α and β results in a significant error.

According to equation (9), first, the nondimensional form of elastic modulus ratio (E_f/E_s) versus density ratio ($\lambda = \rho_f/\rho_s$) was plotted. Then, based on the average values of experimental elastic modulus, regression analysis was performed to calculate the best values of the two constants

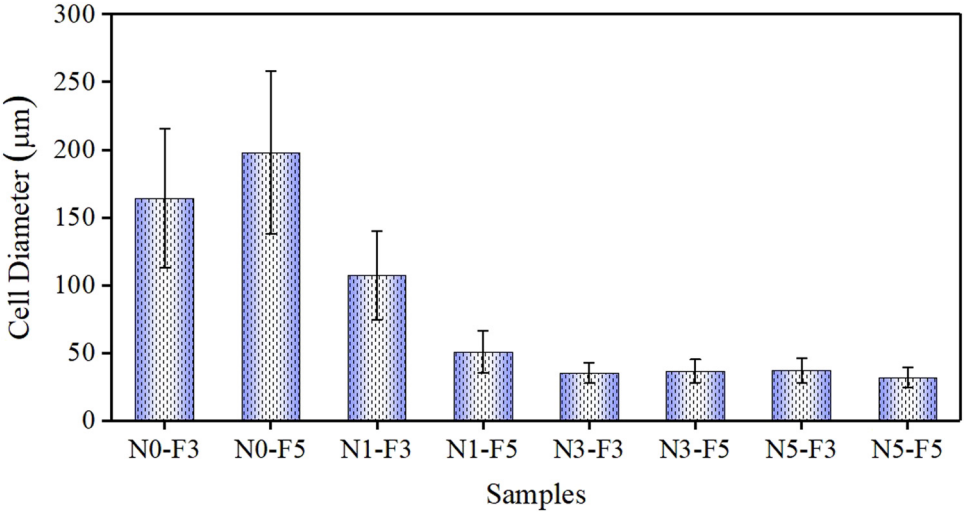

Figure 5: Foams average cell size.

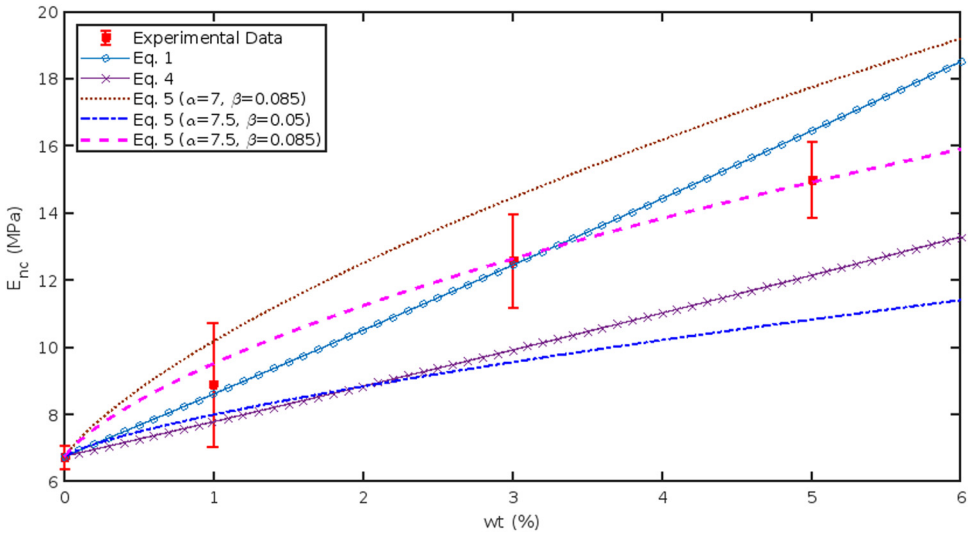

Figure 6: Comparison of the elastic modulus of solid TPU/MWCNT nanocomposites obtained from theoretical approaches with the results obtained from experimental tests with their standard deviations at various MWCNT weight percentages.

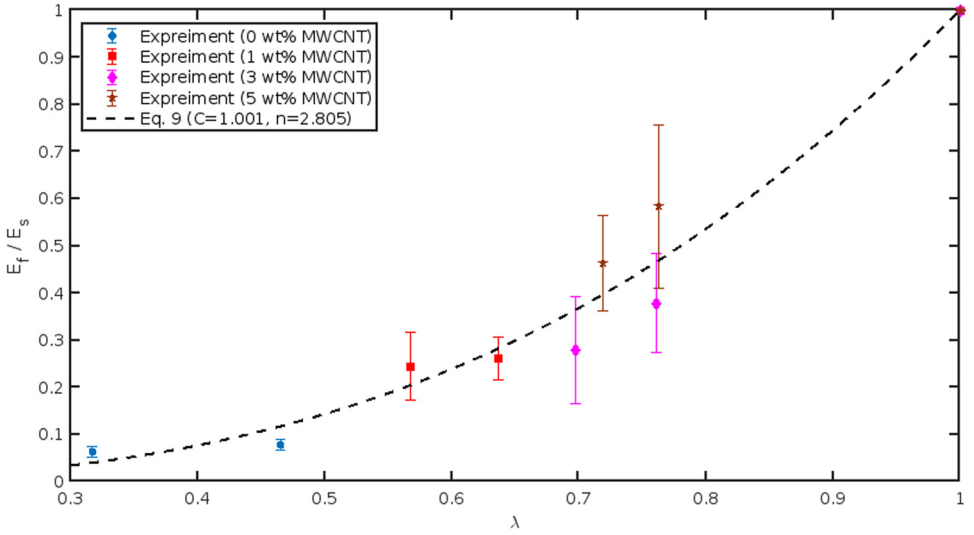

Figure 7: Comparison of the elastic modulus ratio of porous TPU/MWCNT nanocomposites obtained from the theoretical approach with the results obtained from experimental tests at various density ratios.

(C and n) in equation (9). Figure 7 shows the elastic modulus ratio versus density ratio of porous TPU/MWCNT nanocomposites obtained from experimental tests and regression analysis for 0, 1, 3, and 5 wt% of MWCNT. The regression analysis shows that by selecting C = 1.001 and n = 2.805, equation (9) can successfully predict the elastic modulus of such nanocomposite foams regardless of how much MWCNT is involved. The comparison illustrates that except for highly porous pure polymeric materials, which have the lowest elastic modulus, the elastic modulus predictions are properly within the standard deviation values of experimental data. It is worth mentioning that the R-squared value for this regression analysis is R^2 = 0.9766. Moreover, it can be concluded that higher amounts of MWCNTs lead to the formation of foams with lower porosities, which is helpful in improving elastic modulus.

5 Conclusion

This study aimed to fabricate foam TPU/MWCNT nanocomposites with varying MWCNT and CBA contents, using an

industrially scalable foaming method, to enhance their mechanical properties. In conclusion, the results indicated that:

- Increasing the MWCNT content improved the elastic moduli of both the foams and solid TPU/MWCNT.
- The pristine foams and nanocomposite foams demonstrated higher void fraction values in samples with higher CBA content.
- Introduction of MWCNTs into the polymer matrix resulted in a reduction in foam porosity and cell sizes of the nanocomposite foams containing both 3 and 5 wt% chemical CBAs, up to a MWCNT content of 3 wt%.
- The modified HT model successfully estimated Young's modulus of solid nanocomposites by including more MWCNT parameters such as aspect ratio, agglomeration state, waviness, and orientation.
- Gibson and Ashby's method was utilized to determine the best equation for estimating the elastic modulus of pure and nanocomposite TPU foams at a wide range of MWCNT and CBA contents.

Acknowledgments: The work described in this article was supported by the Natural Sciences and Engineering Research Council of Canada (NSERC under grant no. RGPIN-217525). The authors are grateful for their support.

Funding information: This work was supported and funded by the Natural Sciences and Engineering Research Council of Canada (NSERC under grant no. RGPIN-217525).

Author contributions: All authors have accepted responsibility for the entire content of this manuscript and approved its submission.

Conflict of interest: The authors state no conflict of interest.

Data availability statement: The raw/processed data required to reproduce these findings cannot be shared at this time as the data also forms part of an ongoing study.

References

[1] Cai JH, Li J, Chen XD, Wang M. Multifunctional polydimethylsiloxane foam with multi-walled carbon nanotube and thermo-expandable microsphere for temperature sensing, microwave shielding and piezoresistive sensor. Chem Eng J. 2020;393(December 2019):124805.

[2] Chen Z, Sun YC, Wang J, Qi HJ, Wang T, Naguib HE. Flexible, reconfigurable, and self-healing TPU/vitrimer polymer blend with copolymerization triggered by bond exchange reaction. ACS Appl Mater Interfaces. 2020;12(7):8740–50.

[3] Behdinan K, Moradi-Dastjerdi R. Thermal buckling resistance of a lightweight lead-free piezoelectric nanocomposite sandwich plate. Adv Nano Res. 2022;12(6):593–603.

[4] Moradi-Dastjerdi R, Behdinan K. Biaxial buckling analysis of an innovative active sandwich plate. Mech Based Des Struct Mach. 2024;52(1):275–88. doi: 10.1080/15397734.2022.2107539.

[5] Moradi-Dastjerdi R, Behdinan K. Electromechanical natural frequency analysis of an eco-friendly active sandwich plate. Actuators. 2022;11:261. doi: 10.3390/act11090261.

[6] Oh JY, Rondeau-Gagné S, Chiu YC, Chortos A, Lissel F, Wang GJN, et al. Intrinsically stretchable and healable semiconducting polymer for organic transistors. Nature. 2016;539(7629):411–5.

[7] Rogers JA, Someya T, Huang Y. Materials and mechanics for stretchable electronics. Science (80-). 2010;327(5973):1603–7.

[8] Zhou X, Zhu L, Fan L, Deng H, Fu Q. Fabrication of highly stretchable, washable, wearable, water-repellent strain sensors with multi-stimuli sensing ability. ACS Appl Mater Interfaces. 2018;10(37):31655–63.

[9] Hu C, Behdinan K, Moradi-Dastjerdi R. PVDF energy harvester for prolonging the battery life of cardiac pacemakers. Actuators. 2022;11(7):187. doi: 10.3390/act11070187.

[10] Meschino M, Wang L, Xu H, Moradi-Dastjerdi R, Behdinan K. Low-frequency nanocomposite piezoelectric energy harvester with embedded zinc oxide nanowires. Polym Compos. 2021;42:4573–85. doi: 10.1002/pc.26169.

[11] Angelou A, Norman C, Miran N, Albers S, Moradi-Dastjerdi R, Behdinan K. An eco-friendly, biocompatible and reliable piezoelectric nanocomposite actuator for the new generation of microelectronic devices. Eur Phys J Plus. 2021;136:678. doi: 10.1140/epjp/s13360-021-01653-z.

[12] Wang Y, Wang L, Yang T, Li X, Zang X, Zhu M, et al. Wearable and highly sensitive graphene strain sensors for human motion monitoring. Adv Funct Mater. 2014;24(29):4666–70.

[13] Choi DY, Kim MH, Oh YS, Jung SH, Jung JH, Sung HJ, et al. Highly stretchable, hysteresis-free ionic liquid-based strain sensor for precise human motion monitoring. ACS Appl Mater Interfaces. 2017;9(2):1770–80.

[14] Christianson C, Goldberg NN, Deheyn DD, Cai S, Tolley MT. Translucent soft robots driven by frameless fluid electrode dielectric elastomer actuators. Sci Robot. 2018;3(17):1–9.

[15] Acome E, Mitchell SK, Morrissey TG, Emmett MB, Benjamin C, King M, et al. Hydraulically amplified self-healing electrostatic actuators with muscle-like performance. Science (80-). 2018 Jan 5;359(6371):61–5. https://www.science.org/doi/10.1126/science.aao6139.

[16] Wang Q, Jian M, Wang C, Zhang Y. Carbonized silk nanofiber membrane for transparent and sensitive electronic skin. Adv Funct Mater. 2017;27(9):1605657.

[17] Gerratt AP, Michaud HO, Lacour SP. Elastomeric electronic skin for prosthetic tactile sensation. Adv Funct Mater. 2015;25(15):2287–95.

[18] Mahdinejad Gorji J, Payganeh G, Moradi-Dastjerdi R. Mechanical and energy absorption behavior of an innovative high-performance auxetic structure. Mech Based Des Struct Mach. 2024;52(4):2316–35. doi: 10.1080/15397734.2023.2177863.

[19] Ghahramani P, Behdinan K, Naguib HE. Development of piezoresistive PDMS/MWCNT foam nanocomposite sensor with ultrahigh flexibility and compressibility. J Intell Mater Syst Struct. 20211045389X2110643 .

[20] Wan F, Tran MP, Leblanc C, Béchet E, Plougonven E, Léonard A, et al. Experimental and computational micro-mechanical investigations of compressive properties of polypropylene/multi-walled carbon nanotubes nanocomposite foams. Mech Mater. 2015;91(P1):95–118.
[21] Sheikh T, Sampath S, Bhattacharya B. Bimorph sensor based in-line inspection method for corrosion defect detection in natural gas pipelines. Sens Actuators A Phys. 2022;347:113940.
[22] Ding Y, Xu T, Onyilagha O, Fong H, Zhu Z. Recent advances in flexible and wearable pressure sensors based on piezoresistive 3D monolithic conductive sponges. ACS Appl Mater Interfaces. 2019;11(7):6685–704.
[23] Zhao H, Zhang Y, Bradford PD, Zhou Q, Jia Q, Yuan FG, et al. Carbon nanotube yarn strain sensors. Nanotechnology. 2010;21:305502.
[24] Tung TT, Robert C, Castro M, Feller JF, Kim TY, Suh KS. Enhancing the sensitivity of graphene/polyurethane nanocomposite flexible piezo-resistive pressure sensors with magnetite nano-spacers. Carbon N Y. 2016;108:450–60.
[25] Zang Y, Zhang F, Di CA, Zhu D. Advances of flexible pressure sensors toward artificial intelligence and health care applications. Mater Horiz. 2015;2(2):140–56.
[26] Petrossian G, Hohimer CJ, Ameli A. Highly-loaded thermoplastic polyurethane/lead zirconate titanate composite foams with low permittivity fabricated using expandable microspheres. Polymers (Basel). 2019;11(2):280.
[27] Moradi-Dastjerdi R, Behdinan K. Damped harmonic vibrations of axisymmetric graphene-enhanced cylinders in thermal environment. Polym Compos. 2021;42(11):5763–73. doi: 10.1002/pc.26258.
[28] Sheikh T, Behdinan K. Insight of discrete scale and multiscale methods for characterization of composite and nanocomposite materials. Arch Comput Methods Eng. 2023 [cited 2022 Nov 2];30:1231–65. doi: 10.1007/s11831-022-09840-6.
[29] Moradi-Dastjerdi R, Behdinan K. Thermo-electro-mechanical behavior of an advanced smart lightweight sandwich plate. Aerosp Sci Technol. 2020;106:106142. doi: 10.1016/j.ast.2020.106142.
[30] Sheikh T, Behdinan K. The effect of process parameters on the mechanical properties of additively manufactured parts using a hierarchical multiscale model. Rapid Prototyp J. 2023;29(5):1029–43. doi: 10.1108/RPJ-08-2022-0248.
[31] Thompson MR, Motlagh GH, Oxby KJ, Hrymak AN. Multiple percolation in a carbon-filled polymer composites *via* foaming. J Appl Polym Sci. 2010;115(2):646–54.
[32] Huang W, Dai K, Zhai Y, Liu H, Zhan P, Gao J, et al. Flexible and lightweight pressure sensor based on carbon nanotube/thermoplastic polyurethane-aligned conductive foam with superior compressibility and stability. ACS Appl Mater Interfaces. 2017;9(48):42266–77.
[33] Tang Y, Guo Q, Chen Z, Zhang X, Lu C. In-situ reduction of graphene oxide-wrapped porous polyurethane scaffolds: Synergistic enhancement of mechanical properties and piezoresistivity. Compos Part A Appl Sci Manuf. 2019;116(October 2018):106–13.
[34] Kim JS, Kim GW. Hysteresis compensation of piezoresistive carbon nanotube/polydimethylsiloxane composite-based force sensors. Sensors (Switzerland). 2017;17(2):229.
[35] Iglio R, Mariani S, Robbiano V, Strambini L, Barillaro G. Flexible polydimethylsiloxane foams decorated with multiwalled carbon nanotubes enable unprecedented detection of ultralow strain and pressure coupled with a large working range. ACS Appl Mater Interfaces. 2018;10(16):13877–85.
[36] Cao CF, Zhang GD, Zhao L, Gong LX, Gao JF, Jiang JX, et al. Design of mechanically stable, electrically conductive and highly hydrophobic three-dimensional graphene nanoribbon composites by modulating the interconnected network on polymer foam skeleton. Compos Sci Technol. 2019;171(August 2018):162–70.
[37] Chen Q, Cao PF, Advincula RC. Mechanically robust, ultraelastic hierarchical foam with tunable properties *via* 3D printing. Adv Funct Mater. 2018;28(21):1–9.
[38] Yao HB, Ge J, Wang CF, Wang X, Hu W, Zheng ZJ, et al. A flexible and highly pressure-sensitive graphene-polyurethane sponge based on fractured microstructure design. Adv Mater. 2013;25(46):6692–8.
[39] Patole SP, Reddy SK, Schiffer A, Askar K, Prusty BG, Kumar S. Piezoresistive and mechanical characteristics of graphene foam nanocomposites. ACS Appl Nano Mater. 2019;2(3):1402–11.
[40] Boland CS, Khan U, Binions M, Barwich S. Graphene-coated polymer foams as tuneable impact sensors. Nanoscale. 2018;10:5366–75.
[41] Liu H, Dong M, Huang W, Gao J, Dai K, Guo J, et al. Lightweight conductive graphene/thermoplastic polyurethane foams with ultrahigh compressibility for piezoresistive sensing. J Mater Chem C. 2017;5(1):73–83.
[42] Ghahramani P, Eldyasti A, Leung SN. Open-cell polyvinylidene fluoride foams as carriers to promote biofilm growth for biological wastewater treatment. Polym Eng Sci. 2021 Aug 1 [cited 2021 Aug 13];61(8)2161–71. https://onlinelibrary.wiley.com/doi/full/10.1002/pen.25741.
[43] Ghahramani P. Design and fabrication of open-cell foams for biological organic removal from wastewater. MSc Thesis. Toronto, Canada: York University; 2018.
[44] Matuana LM, Faruk O. Effect of gas saturation conditions on the expansion ratio of microcellular poly(lactic acid)/wood-flour composites. Express Polym Lett. 2010;4(10):621–31. http://www.expresspolymlett.com/letolt.php?file=EPL-0001615&mi=c.
[45] Xu D, Pop-Iliev R, Park CB, Fenton RG. Fundamental study of CBA-blown bubble growth and collapse under atmospheric pressure. J Cell Plast. 2005;41(6):519–38.
[46] Damanpack AR, Sousa A, Bodaghi M. Porous plas with controllable density by fdm 3d printing and chemical foaming agent. Micromachines. 2021;12(8):1–8.
[47] Chung CY, Hwang SS, Chen SC, Lai MC. Effects of injection molding process parameters on the chemical foaming behavior of polypropylene and polystyrene. Polymers (Basel). 2021;13(14):2331.
[48] Yamsaengsung W, Sombatsompop N. Effect of chemical blowing agent on cell structure and mechanical properties of EPDM foam, and peel strength and thermal conductivity of wood/NR composite-EPDM foam laminates. Compos Part B Eng. 2009;40(7):594–600.
[49] Ameli A, Nofar M, Park CB, Pötschke P, Rizvi G. Polypropylene/carbon nanotube nano/microcellular structures with high dielectric permittivity, low dielectric loss, and low percolation threshold. Carbon N Y. 2014;71:206–17.
[50] Boubakri A, Guermazi N, Elleuch K, Ayedi HF. Study of UV-aging of thermoplastic polyurethane material. Mater Sci Eng A. 2010;527(7–8):1649–54.
[51] Kim JH, Kim GH. Effect of rubber content on abrasion resistance and tensile properties of thermoplastic polyurethane (TPU)/rubber blends. Macromol Res. 2014;22(5):523–7.
[52] Singh NP, Gupta VK, Singh AP. Graphene and carbon nanotube reinforced epoxy nanocomposites: A review. Polymer (Guildf). 2019

Oct [cited 2019 Oct 4];180:121724. https://www.sciencedirect.com/science/article/pii/S003238611930730X.
[53] Moradi-Dastjerdi R, Behdinan K. Dynamic performance of piezoelectric energy harvesters with a multifunctional nanocomposite substrate. Appl Energy. 2021;293:116947. doi: 10.1016/j.apenergy.2021.116947.
[54] Ghahramani P, Behdinan K, Moradi-Dastjerdi R, Naguib HE. Theoretical and experimental investigation of MWCNT dispersion effect on the elastic modulus of flexible PDMS/MWCNT nanocomposites. Nanotechnol Rev. 2022;11:55–64. doi: 10.1515/ntrev-2022-0006.
[55] Pan S, Feng J, Safaei B, Qin Z, Chu F, Hui D. A comparative experimental study on damping properties of epoxy nanocomposite beams reinforced with carbon nanotubes and graphene nanoplatelets. Nanotechnol Rev. 2022 Jan [cited 2022 Aug 12];11(1):1658–69, https://www.degruyter.com/document/doi/10.1515/ntrev-2022-0107/html.
[56] Ghahramani P, Moradi-Dastjerdi R, Behdinan K, Naguib HE. Mechanical characterization of multifunctional highly porous carbon nanotube-reinforced foams. Polym Compos. 2023;44(4):2093–101. doi: 10.1002/pc.27226.
[57] Chang E, Ameli A, Alian AR, Mark LH, Yu K, Wang S, et al. Percolation mechanism and effective conductivity of mechanically deformed 3-dimensional composite networks: Computational modeling and experimental verification. Compos Part B Eng. 2021;207(December 2020):108552. doi: 10.1016/j.compositesb.2020.108552.
[58] Tanabe F, Yoshimoto S, Noda Y, Araki T, Uemura T, Takeuchi Y, et al. Flexible sensor sheet for real-time pressure monitoring in artificial knee joint during total knee arthroplasty. 39th Annu Int Conf IEEE Eng Med Biol Soc EMBS; 2017. p. 1591–4.
[59] Fei Y, Jiang R, Fang W, Liu T, Saeb MR, Hejna A, et al. Highly sensitive large strain cellulose/multiwalled carbon nanotubes (MWCNTs)/thermoplastic polyurethane (TPU) nanocomposite foams: From design to performance evaluation. J Supercrit Fluids. 2022;188(June):105653.
[60] Moore B, Jaglinski T, Stone DS, Lakes RS. On the bulk modulus of open cell foams. Cell Polym. 2007;26(1):1–10.
[61] Gui X, Cao A, Wei J, Li H, Jia Y, Li Z, et al. Soft, highly conductive nanotube sponges and composites with controlled compressibility. ACS Nano. 2010;4(4):2320–6.
[62] Rinaldi A, Tamburrano A, Fortunato M, Sarto MS. A flexible and highly sensitive pressure sensor based on a PDMS foam coated with graphene nanoplatelets. Sensors (Switzerland). 2016;16(12):2148.
[63] Hou Q, Grijpma DW, Feijen J. Porous polymeric structures for tissue engineering prepared by a coagulation, compression moulding and salt leaching technique. Biomaterials. 2003;24(11):1937–47.
[64] Thilagashanthi T, Gunasekaran K, Satyanarayanan KS. Microstructural pore analysis using SEM and ImageJ on the absorption of treated coconut shell aggregate. J Clean Prod. 2021;324:129217. doi: 10.1016/j.jclepro.2021.129217.
[65] Yunus S, Sefa-Ntiri B, Anderson B, Kumi F, Mensah-Amoah P, Sackey SS. Quantitative pore characterization of polyurethane foam with cost-effective imaging tools and image analysis: A proof-of-principle study. Polymers (Basel). 2019;11(11):1879.
[66] Gibson LJ, Ashby MF. The mechanics of foams: basic results. In: Cellular solids: Structure and properties. 2nd edn. Cambridge: Cambridge University Press; 1997. p. 175–234.
[67] Moradi-Dastjerdi R, Behdinan K. Stress waves in a lightweight substrate plate actuated with piezoelectric layers under sinusoidal time-dependent pressures. Aerosp Sci Technol. 2023;132:108057. doi: 10.1016/j.ast.2022.108057.
[68] Behdinan K, Moradi-Dastjerdi R. Advanced multifunctional lightweight aerostructures: Design, development, and implementation. In: Behdinan K, Moradi-Dastjerdi R, editors. 1st edn. Hoboken: John Wiley & Sons Ltd; 2021. p. 256. https://onlinelibrary.wiley.com/doi/book/10.1002/9781119756743.
[69] Moradi-Dastjerdi R, Sheikhi MM, Shamsolhoseinian HR. Stress distribution in functionally graded nanocomposite cylinders reinforced by wavy carbon nanotube. Int J Adv Des Manuf Technol. 2014;7(4):43–54.
[70] Kundalwal SI. Review on micromechanics of nano- and micro-fiber reinforced composites. Polym Compos. 2018;39(12):4243–74. doi: 10.1002/pc.24569.
[71] Shokrieh MM, Rafiee R. Investigation of nanotube length effect on the reinforcement efficiency in carbon nanotube based composites. Compos Struct. 2010;92:2415–20.
[72] Georgantzinos SK, Markolefas SI, Mavrommatis SA, Stamoulis KP. Finite element modelling of carbon fiber-carbon nanostructure-polymer hybrid composite structures. In MATEC Web of Conference. 2020 [cited 2022 Sep 23]. p. 314. doi: 10.1051/matecconf/202031402004.
[73] Kazem Hassanzadeh-Aghdam M, Jamali J. A new form of a Halpin-Tsai micromechanical model for characterizing the mechanical properties of carbon nanotube-reinforced polymer nanocomposites. Bull Mater Sci. 2019;42:117. doi: 10.1007/s12034-019-1784-6.
[74] Georgantzinos SK, Antoniou P, Markolefas S, Giannopoulos G. Finite element predictions on vibrations of laminated composite plates incorporating the random orientation, agglomeration, and waviness of carbon nanotubes Agglomeration factor of CNTs f mn Natural frequency (Hz) G Shear modulus h Total plate thickness. Acta Mech. 2022 [cited 2022 Sep 21];233:2031–59. doi: 10.1007/s00707-022-03179-6.
[75] Cox HL. The elasticity and strength of paper and other fibrous materials. Br J Appl Phys. 1952 Mar [cited 2022 Sep 23];3(3):72. https://iopscience.iop.org/article/10.1088/0508-3443/3/3/302.
[76] Omidi M, Hossein Rokni DT, Milani AS, Seethaler RJ, Arasteh R. Prediction of the mechanical characteristics of multi-walled carbon nanotube/epoxy composites using a new form of the rule of mixtures. Carbon N Y. 2010;48(11):3218–28.
[77] Fisher FT, Bradshaw RD, Brinson LC. Fiber waviness in nanotube-reinforced polymer composites — I: Modulus predictions using effective nanotube properties. Compos Sci Technol. 2003;63:1–15.
[78] Roberts AP, Garboczi EJ. Elastic moduli of model random three-dimensional closed-cell cellular solids. Acta Mater. 2001 Jan 22;49(2):189–97.
[79] Farsheh AT, Talaeipour M, Hemmasi AH, Khademieslam H, Ghasemi I. Investigation on the mechanical and morphological properties of foamed nanocomposites based on wood flour/PVC/multi-walled carbon nanotube. BioResources. 2011;6(1):841–52.